Ceramics International 49 (2023) 30501–30509

Contents lists available at ScienceDirect

Ceramics International

journal homepage: www.elsevier.com/locate/ceramint

Synthesis of WO_3 nanopowder using a green surfactant for efficient gas sensing applications

Hakimeh Pakdel [a,1], Vardan Galstyan [a,b,*,1], Annalisa D'Arco [c,d], Tiziana Mancini [c], Stefano Lupi [c,d], Abderrahim Moumen [a,e], Matteo Borsi [a], Elisabetta Comini [a,**]

[a] Sensor Lab, Department of Information Engineering, University of Brescia, Via Valotti 9, 25133, Brescia, Italy
[b] Department of Engineering "Enzo Ferrari", University of Modena and Reggio Emilia, Via Vivarelli 10, 41125, Modena, Italy
[c] Physics Department, University of Rome 'La Sapienza', P.le A. Moro 5, 00185, Rome, Italy
[d] INFN-LNF Via E, Fermi 40, 00044, Frascati, Italy
[e] Department of Mathematical, Physical and Computer Sciences, University of Parma, Parco Area delle Scienze 7/A, 43124, Parma, Italy

ARTICLE INFO

Keywords:
WO_3 nanopowder
Eco-friendly synthesis
Green surfactant
Chemical gas sensor
Selective detection
Environmental monitoring

ABSTRACT

WO_3 has attracted great attention for chemical gas sensing applications. However, the synthesis of WO_3 is mainly performed by using hazardous organic solvents and corrosive acidic solutions, which can result in environmental and health issues. The development of safe synthesis procedures using green compounds and solvents is in great demand to overcome the aforementioned drawbacks. Therefore, the effect of different eco-friendly chemical compounds on the growth of WO_3 materials has yet to be thoroughly studied. Meanwhile, the fabrication of material at the nanoscale with specific crystalline properties may improve its sensitivity to the target gas. In this work, we report an efficient method for the synthesis of WO_3 nanopowder by using water and a green surfactant such as vitamin C. The growth mechanism of the structure is analyzed considering the nature of solutions and surfactants. The studies indicate that the surfactant has a crucial effect on the formation of nanoparticles. Furthermore, the experimental findings show that the fabricated monoclinic WO_3 material is highly sensitive and selective to low concentrations of acetone. Moreover, the structure exhibits quite stable functionalities at different levels of environmental humidity. Hence, this work may have a considerable impact on the existing techniques for the preparation of WO_3 nanomaterials providing new insights into their green synthesis procedures. In addition, it can significantly affect the development of high-performance gas sensors and other catalytic devices based on WO_3 nanostructures.

1. Introduction

Nowadays, green chemistry is highly required to reduce the use and production of hazardous substances. In this respect, green synthesis methods are designed considering twelve basic principles of green chemistry [1–3]. Therein, the fabrication of nanostructured materials without using dangerous organic solvents, corrosive acids (for example, HNO_3, HCl, or H_2SO_4), or non-toxic reagents is one of the most significant challenges to minimizing the application of harmful substances [1,4–8]. Moreover, particular attention should be paid to the enhancement of the efficiency of chemical processes [3,9].

Intensive studies have been carried out to explore green technological procedures for preparing semiconductor nanostructures with different shapes and their application in energy, medicine, and sensing [8,10–12]. Especially, the large surface area of nanomaterials and the possibility of tailoring their composition and structure make them very attractive candidates for application in chemical gas sensors. Here, the enhancement of the material surface area will affect its interaction with gaseous compounds, while the compositional and structural modifications can improve its reactivity to specific gaseous or volatile compounds [13–15]. The need for high-performance chemical gas sensors based on semiconductor nanomaterials is justified by several factors, such as indoor and outdoor air quality monitoring, safety in industrial processes, and health status diagnosis [16–19]. Therefore, the

* Corresponding author. Sensor Lab, Department of Information Engineering, University of Brescia, Via Valotti 9, 25133, Brescia, Italy.
** Corresponding author.
E-mail addresses: vardan.galstyan@unibs.it (V. Galstyan), elisabetta.comini@unibs.it (E. Comini).
[1] These authors contributed equally.

https://doi.org/10.1016/j.ceramint.2023.06.314
Received 8 April 2023; Received in revised form 19 June 2023; Accepted 27 June 2023
Available online 4 July 2023

integration of eco-friendly synthesis procedures into the development of chemiresistive gas sensors has received considerable attention [13,20]. Different chemical approaches have been used for the green synthesis of metal oxide nanomaterials. However, oxide nanostructures have a high tendency to agglomerate, and avoiding this phenomenon is crucial for their preparation [7,21–23].

As an n-type oxide semiconductor, WO_3 has been employed in various applications owing to its unique physical and chemical characteristics such as high stability, biocompatibility, nontoxicity, and low cost [24–26]. The experimental and theoretical investigations suggest that WO_3 is an attractive material for its application in chemical gas sensing devices [27–31]. However, the green synthesis of WO_3 nanostructures is in its infancy, and therefore the effect of different approaches, chemicals, and solvents on structure growth should be examined to identify the optimum methods and materials to be used. Recent achievements in green synthesis procedures show that metal oxide nanostructures can be prepared using different biomolecules like vitamins, proteins, amino acids, organic acids, and polyphenols, which can be extracted from other plants and act as structure-directing agents [7,23,24,32]. Among the fabrication techniques, the precipitation approach provides a flexible and cost-effective tool for producing nanomaterials at relatively low temperatures and controlling their morphology, porosity, and size [33–35].

In this paper, we report a simple, low-cost, and environmentally friendly approach for the fabrication of WO_3 nanopowder in the aqueous medium using vitamin C as a surfactant. The morphology of the material is studied by field-emission scanning electron microscopy (FESEM). The structure and the chemical composition are analyzed by X-ray diffraction (XRD), Raman, and attenuated total reflectance (ATR) Fourier-transform infrared (IR) spectroscopy. Experimental findings indicate the fabrication of powdered material with individual nanoparticles. Meanwhile, the surfactant nature is crucial for the formation of well-defined particles. Chemical gas sensing investigations show that the material has a good and selective response to acetone molecules. Furthermore, the monoclinic crystal structure of prepared WO_3 significantly affects its sensing performance. Thus, the results of this research study can be employed in green technologies for the synthesis of WO_3 nanomaterials, as well as in the fabrication of gas sensors and other catalytic systems.

2. Experimental

2.1. Synthesis of powders

WO_3 nanopowders were synthesized by the precipitation method in different solutions, where tungsten (VI) chloride (WCl_6, Sigma-Aldrich) was used as the precursor material. Vitamin C was obtained from Sigma-Aldrich. Potassium sulfate was obtained from Fluka. The solutions were prepared in distilled water (Carlo Erba Reagents) with three different compositions.

(i) 1 g of WCl_6 was dissolved in 50 ml of distilled water (H_2O) and stirred for 5 h at room temperature.
(ii) Aqueous solution of vitamin C was prepared as follows: 1 M aqueous solution of vitamin C was stirred for 20 min at room temperature. Then, WCl_6 was dissolved in 50 ml of H_2O and stirred for 30 min at room temperature. Afterward, 1 M solution of vitamin C was added dropwise into the precursor solution (WCl_6/H_2O) until the pH value reached 2 and stirred for 5 and 24 h. Herein, vitamin C was used as the green capping, reducing, and pH control agent.
(iii) The third solution was prepared as the second one, however, instead of 1 M vitamin C, 0.8 M potassium sulfate was added to the solution as the structure-directing agent.

After the preparation procedure, the resulting solutions were kept at room temperature for 2 h allowing them to settle out. The precipitates were collected by centrifugation. Then, the salt ions as well as the other side-products were removed from precipitates by washing them with H_2O and ethanol. The final powders were dried at room temperature for 24 h and then annealed at 450 °C for 2 h.

2.2. Characterizations

The morphological properties of fabricated materials were investigated using high-resolution FESEM (MIRA3 FEG-SEM, TESCAN). The structural properties were analyzed by XRD (Empyrean model, PANalytical, The Netherlands) with a Cu-LFF ($\lambda = 1.54$ Å) source at 40 kV and 40 mA. The 2θ (Bragg's diffraction angles) measurements were carried out from 15° to 90° with a scan speed of 100 s and a step size of 0.013°.

Raman spectra were recorded by a Jasco NRS-5100 confocal Raman microscope equipped with the excitation laser diode (wavelength: 785 nm, grating: 600 l/mm) that operates at a nominal power of 20 mW. An MPLFLN 100x objective focuses the laser beam on the sample with a 1 μm spot and the backscattered signal is collected using a cooled (−69 °C) CCD camera. The studies were carried out in the range of 50–1800 cm^{-1} with an effective power of 6.0 mW, an accumulation number of 50, an exposure value of 7 s, and a resolution of 2 cm^{-1}. Four spectral measurements were performed for the synthesized material and spectra have been processed (baseline correction and data smoothing) with the Spectra Manager™ software (Jasco).

ATR-IR spectra were recorded by the FTIR Vertex 70 interferometer (Bruker Optics, Ettlingen, Germany). The interferometer is equipped with an ATR crystal module (Bruker-Diamond single reflection crystal) with a single reflection diamond crystal at 45°, a thermal source (Globar), and a wide-range RT-DLaTGS detector. The measurements were carried out in a vacuum. The ATR-IR spectra of WO_3 powder were acquired with an acquisition rate of 7.5 kHz in the spectral region of 50–6000 cm^{-1} by averaging 128 scans with a spectral resolution of 4 cm^{-1}. Second-derivative analyses were performed both for the Raman and for the ATR-IR spectra by applying a 13-point smoothing filter [36]. Post-processing data analysis and visualization were performed using OPUS™ 8.2 software (Bruker) and OriginPro™ 9.0, respectively.

2.3. Fabrication of WO_3 sensor device

To study the sensing properties of the synthesized nanopowder, the alumina substrates (99.9% purity, 2 mm × 2 mm, Kyocera, Japan) were cleaned by sonication in acetone, ethanol, and H_2O. Afterward, TiW adhesion films and platinum interdigitated electrodes were deposited on the alumina substrates by means of DC magnetron sputtering at a power of 70 W, 7 SCCM argon flow, and 5.1×10^{-3} mbar pressure in the sputtering chamber. A platinum heater was deposited on the backside of the substrates to control the operating temperature of the sensing structure (Fig. S1). Then, the fabricated WO_3 powder was dispersed in H_2O and sonicated for 10 min. The resulting dispersion was drop-casted on alumina substrates using a dispenser (Gilson Company, France). We made a cut of the substrate to show the thickness of the WO_3 nanostructure after the drop-casting of the aqueous dispersion of nanoparticles (Fig. S2). As-prepared materials were annealed at 450 °C to stabilize their crystalline and electrical properties at high operating temperatures. Therefore, we chose 400 °C as the maximum temperature for gas sensing studies. Sensing analyses were carried out in a thermostatic test chamber, where the humidity level is kept under control using a humidity sensor. A detailed description of the system for gas sensing measurements has been reported previously [37].

The sensing response of the WO_3 structure toward reducing gases was calculated according to Eqn (1):

$$\frac{(G_f - G_0)}{G_0} = \frac{\Delta G}{G_0} \quad (1)$$

Here, G_0 is the baseline conductance of the WO_3 sensor in air and G_f is the steady-state conductance value of the sensor in the presence of the analyte compound. The response toward an oxidizing gase was calculated according to Eqn (2), where R_0 is the baseline resistance of the WO_3 in air, and R_f is the steady-state resistance of the material in the presence of oxidizing gas.

$$\frac{(R_f - R_0)}{R_0} = \frac{\Delta R}{R_0} \quad (2)$$

3. Results and discussion

3.1. Morphology and structure

Fig. 1 (a–d), (f), and (g) report the FESEM images of the WO_3 materials prepared in H_2O, in the aqueous solutions of vitamin C and potassium sulfate. The morphology of the WO_3 structure synthesized in the surfactant-free aqueous solution with a reaction time of 5 h is shown in Fig. 1 (a) and (b). Herein, agglomeration of particles is observed. Instead, well-defined WO_3 nanoparticles with an average dimension of 52 nm are fabricated in the vitamin C-containing aqueous solution using the same reaction time (Fig. 1 (c–e) and Fig. S3 (a)). The morphology of the material prepared in the aqueous solution of potassium sulfate is shown in Fig. 1 (f) and (g). The obtained results indicate that the WO_3 particles aglomerate.

The agglomeration of WO_3 nanoparticles synthesized in H_2O (Fig. 1 (a) and (b)) can be attributed to the high reactivity of the tungsten precursor (WCl_6) and its rapid hydrolyzation [38]. The morphological observations of the WO_3 structure prepared in the aqueous solution of vitamin C indicate that the latest acts as a mild reducing and capping agent, resulting in uniform growth of WO_3 particles without agglomeration [39,40]. In this case, the organic molecules attach to the growth surface and avoid the agglomeration of nanoparticles owing to the electrostatic or steric stabilization effects. Hence, vitamin C occupies the available growth sites having a significant effect on the formation and size of nanoparticles [41–45]. Furthermore, the application of potassium sulfate as a capping agent partially affects the separation of particles (Fig. 1 (f and g)), which indicates that vitamin C-containing aqueous solution is the most efficient for the synthesis of WO_3 nanoparticles. In the aforementioned experiments, the reaction procedures for the fabrication of precipitates are performed at room temperature, thus reducing power consumption. We propose that the insufficient separation of particles in the aqueous solution of potassium sulfate can be described as follows: due to the low-temperature processing, the capping interaction is not strong enough, and therefore the primary WO_3 nucleus can be formed without controlling the growth mechanism by the capping agent (potassium sulfate) [46]. However, it is worth mentioning that the nanoparticles tend to agglomerate when the reaction time in the solution of vitamin C is increased to 24 h (Fig. S2 (b) and (c)). This can be attributed to the self-assembly effect of the Ostwald ripening

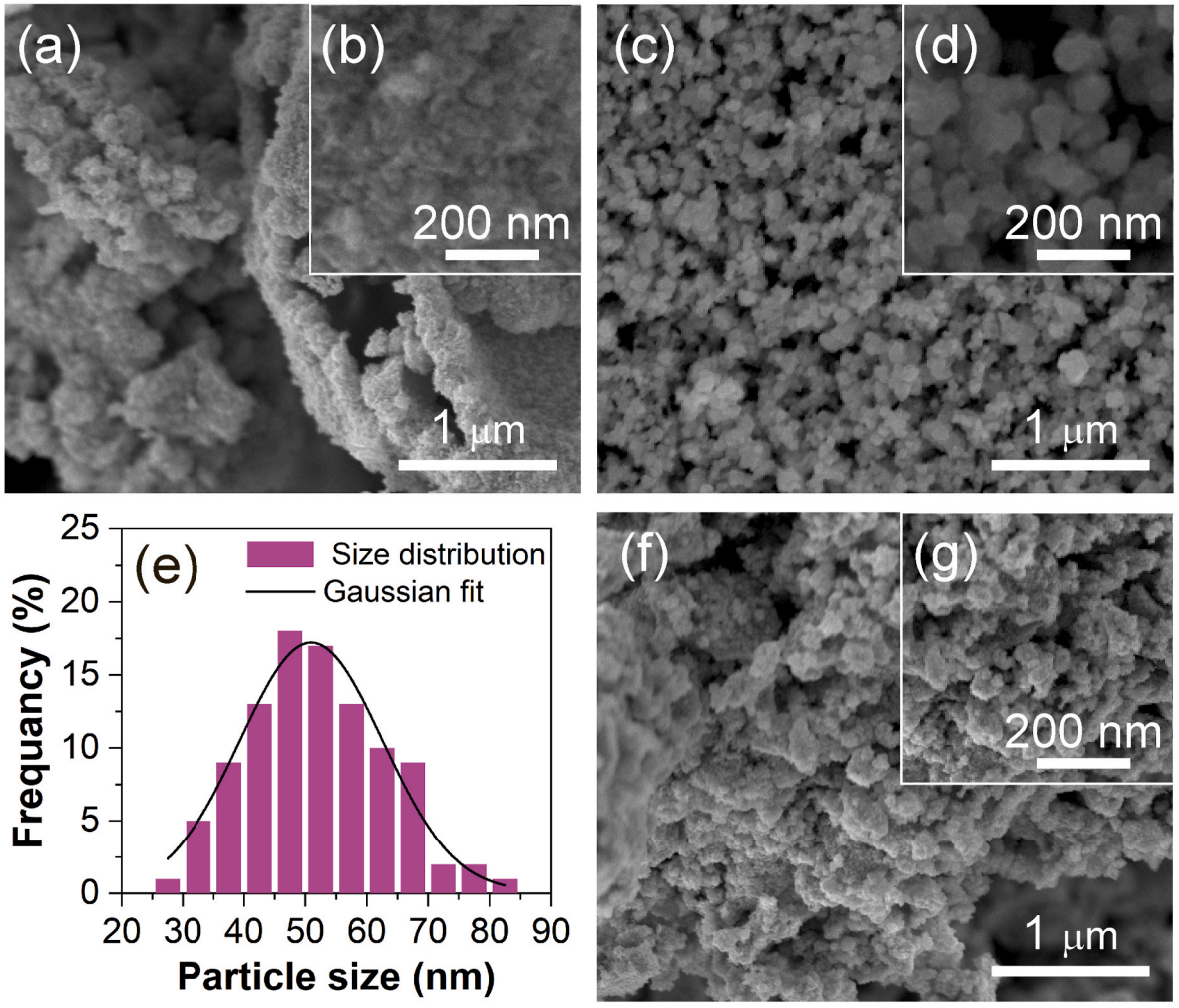

Fig. 1. FESEM images of fabricated WO_3 powders: (a) and (b) Material synthesized in H_2O with a reaction time of 5 h, (c) and (d) WO_3 nanoparticles prepared in vitamin C-containing aqueous solution with a reaction time of 5 h. (e) Particle size distribution histogram of WO_3 powder prepared in the aqueous solution of vitamin C with a reaction time of 5 h. (f) and (g) WO_3 material obtained in potassium sulfate-containing aqueous solutions with a reaction time of 5 h.

mechanism, where small particles dissolve in the solution followed by the formation of bigger ones [47,48]. Therefore, further, we studied the crystalline, compositional, and gas sensing properties of the WO_3 nanopowder synthesized in the aqueous solutions of vitamin C with a reaction time of 5 h (Fig. 1 (c) and (d)). Moreover, vitamin C is a green agent, and thus the preparation of WO_3 nanopowder in the aqueous solution of vitamin C can be considered a green synthesis procedure. Furthermore, previous works used vitamin C with other additives such as hydrochloric acid, urea, oxalic acid, and sodium sulfate, which are not considered environmentally friendly reagents [49–51].

Fig. 2 (a) shows the XRD pattern of the WO_3 powder. The diffraction pattern of the material is matched with the monoclinic phase (JCPDS no. 98-007-1692, space group: P 121/c 1 and space group number: 14). No other phases are detected in this pattern. The main peaks located at 23.175, 23.653, 24.418, 28.843, 33.353, 34.277, 41.707, 50.088, 50.650, and 55.881 are attributed to the (100), (020), (002), (11−1), (120), (02−2), (122), (210), (12−3), and (14−1) planes of monoclinic WO_3, respectively.

The Raman spectrum of the WO_3 powder is reported in Fig. 2 (b). The peak positions and their assignments are listed in Table 1 [52–55]. In particular, every mode can be associated with a crystalline phase or with a hydration state. We mainly compared our results with the detailed studies of Pecquenard et al. [53] and Daniel et al. [52] Generally, the Raman spectrum of WO_3 shows the contribution of deformation lattice mode between 200 and 400 cm^{-1}, stretching modes between 600 and 900 cm^{-1}, and then the contribution of external terminal oxygen bond W═O around 950 cm^{-1} [52–55].

In the spectrum of prepared WO_3 powder, intense Raman resonances are visible around 59, 71, 92, 134, 271, 329, 714, and 805 cm^{-1}. The peak at 71 cm^{-1} and the intense shoulders at 59 and 92 cm^{-1} are due to $(W_2O_2)_n$ chain vibrations in the lattice of WO_3. They are characteristic frequencies of the monoclinic structure [53,54]. The peak located around 270 cm^{-1} can be assigned to O–W–O bending modes of binding oxygen of WO_3 [55]. The weak peak at 188 cm^{-1} is associated with the lattice mode and is characteristic of the monoclinic structure [52]. The sharp bands at 805 cm^{-1} and 714 cm^{-1} can be assigned to the stretching vibration of O–W–O and correspond to the mode of monoclinic WO_3 [52]. The WO_3 powder is synthesized using vitamin C ($C_6H_8O_6$) as a surfactant and H_2O as a solvent. However, residual vitamin C content is not observed in its Raman spectrum.

Considering the Raman peak assignments, the presence of the bands at 59, 71, 92, 133, 188, 221, 270, 329, 436, 714, and 805 cm^{-1} indicate that the prepared powder is mainly crystallized into the monoclinic WO_3. However, we observed very weak shoulders at high frequencies (between 940 cm^{-1} and 960 cm^{-1}) and at low frequencies (at 207 and 375 cm^{-1}), which suggests the presence of a little amount of hydrates.

Fig. 2 (c) shows the ATR-IR spectrum of the fabricated WO_3 powder. The peak positions and assignments of WO_3 powder are reported in Table 2. In the far-IR region, the spectrum shows intense and visible broad bands at around 100 and 189 cm^{-1}, which can be ascribed to the lattice modes of W-oxides. Furthermore, the main IR bands located in the very low-frequency region (around 160, 140, 130, and 110 cm^{-1}) can be ascribed to lattice modes of WO_3. Three bands at 242, 317 and around 338 cm^{-1} correspond to the vibration modes of W–O–W [52, 57–59]. The IR bands at 318–360 cm^{-1} correspond to the W–O–W vibration of WO_3. A shoulder is observed at 394 cm^{-1}, which can be attributed to the (W–OH_2) bending modes of water molecules [57,59].

An intense broad band is observed in the mid-IR spectral region. Its main sharp peak at 616 cm^{-1} and two shoulders around 730 and 757 cm^{-1} can be associated with (W–O) vibrational stretching modes [57, 59]. The other two shoulders, identified with the 2nd derivative analysis, are located at around 867 and 954 cm^{-1} and indexed as stretching modes of (O–W–O) and (W═O), respectively [58,60].

Furthermore, the ATR-IR spectrum of the WO_3 powder showed a very weak band at around 1617 cm^{-1} located in the bending region of H_2O molecules, which could be related to the water content in the

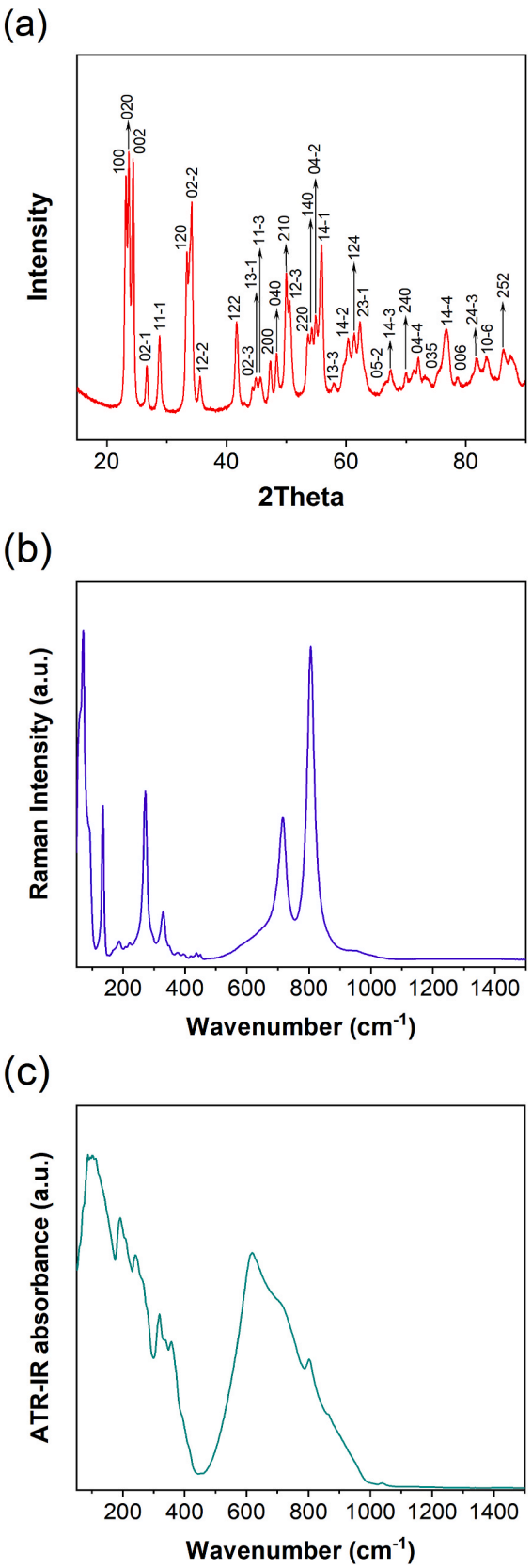

Fig. 2. (a) XRD pattern of the WO_3 nanopowder synthesized in the aqueous solution of vitamin C with a reaction time of 5 h. (b) Raman spectrum of WO_3 powder in the spectral region of 50–1500 cm^{-1}. The whole Raman spectrum is reported in Fig. S4 (a). (c) ATR-IR spectrum of WO_3 in the spectral region between 50 and 1500 cm^{-1}. The whole ATR-IR spectrum is reported in Fig. S4 (b).

Table 1
Raman peak/band positions and chemical group assignment of the fabricated WO_3 powder [52,56,57].

Frequency position cm^{-1}	Assignment
59	ν (W_2O_2)
71	ν(W_2O_2)
92	ν (W_2O_2) Lattice mode
133	Lattice mode
170	–
188	Lattice mode
207	ν (W–O–W)
221	ν (W–O–W)
270	δ (O–W–O)
329	δ (O–W–O) ν (W–OH_2)
375	ν (W–OH_2)
395	//weak shoulder
436	ν (W–OH_2)
714	ν (O–W–O)
805	ν (O–W–O)
954	ν (W═O)

Table 2
Infrared peak/band positions and assignments of WO_3 powder [52, 57–61].

Frequency position (cm^{-1})	Assignment
50	lattice modes
85	lattice modes
100	lattice modes
110	lattice modes
131	–
140	lattice modes
160	lattice modes
189	lattice modes
211	lattice modes
242	ν(W–O–W)
265	ν(W–O–W)
282	δ(O–W–O)
317	ν(W–O–W)
338	ν(W–O–W)
358	ν(W–OH_2)
394	δ(W–OH_2)
417	δ(W–O)
614	–
638	ν(W–O)
726	ν(W–O)
757	ν(O–W–O)
804	
867	ν(O–W–O)
954	ν(W═O)
1012	–
1039	δ(W–OH)
1617	δ (OH)

material [57].

The presence of the main bands at 282, 338, 638, 736, 757, and 867 cm^{-1} can be associated with the monoclinic WO_3 phase [52,56,57], which is in agreement with the results obtained by the Raman measurements.

3.2. Gas sensing results

Fig. 3 (a) reports the sensing response of WO_3 nanoparticles toward 10 ppm of acetone at different operating temperatures (from 200 to 400 °C) and 40% of relative humidity (RH). As is apparent, the response of the material increases with its operating temperature showing the highest response value at 400 °C. Fig. 3 (b) displays the dynamic gas sensing characteristic of the WO_3 sensor at its optimum operating temperature (400 °C). The electrical conductance of the sensor increases due to the injection of each concentration of acetone into the test chamber and returns back to its baseline after the purification of the chamber by synthetic air flow. When the material is exposed to air, the environmental oxygen is adsorbed on its surface trapping electrons from the conduction band and consequently forming oxygen ions (Eqn (3–6)) [62,63].

$$O_2(gas) \leftrightarrow O_2(ads) \quad (3)$$

$$O_2(ads) + e^- \leftrightarrow O_2^-(ads) \quad (4)$$

$$O_2^-(ads) + e^- \leftrightarrow 2O^-(ads) \quad (5)$$

$$O^-(ads) + e^- \leftrightarrow 2O^{2-}(ads) \quad (6)$$

As the sensing structure is exposed to a reducing volatile organic compound such as acetone, the adsorbed oxygen species interact with its molecules (Eqn (7)), and the trapped electrons realize back to the conductance band of the material [64–66]. Hence, the adsorbed acetone acts as an electron donor and increases the conductance of the sensor.

$$CH_3COCH_3(gas) + 8O^- \rightarrow 3CO_2 + 3H_2O + 8e^- \quad (7)$$

Furthermore, the conductance variation behavior of the sensor due to the exposure to acetone and purification of the test chamber indicates the reversible interaction between the acetone and fabricated nanostructure and confirms the n-type conductivity of WO_3 [67]. The adsorption of environmental oxygen on the surface of WO_3 is less efficient at low operating temperatures, which may affect the interaction and exchange process of charge carriers between acetone molecules and the material surface [28,68]. Furthermore, the chemisorption of complex organic molecules of acetone on oxide material requires high activation energy and multi-step reactions between the sensing structure and acetone [31,69]. Therefore, the response of the fabricated WO_3 sensor to acetone strongly depends on its operating temperature and shows an optimum value at 400 °C (Fig. 3(a)).

Response variation of the WO_3 depending on the concentration of acetone (0.2–10 ppm) is demostrated in Fig. 3 (c) and (d) (The response values of the material are reported in Table S1). Here, two linear regions can be observed. Curve-fitting analyses using linear regression show that the slope (2.53) for the low concentrations range (0.2–1 ppm) is larger compared to the one (0.62) for the higher concentrations range (2–10). These findings indicate that the material exhibits a higher sensitivity at low concentrations of acetone. The good response of the material to low concentrations of acetone is a significant achievement because the concentration level of breath acetone for healthy people is lower than 1.8 ppm and for diabetics is higher compared to the aforementioned value [70,71]. Thus, the synthesized material is promising for its application in medical diagnostics and environmental monitoring.

Typically, the properties of chemiresistive sensing structures should be investigated at different levels of humidity, which is very important for their real-life applications. Therefore, we analyzed the functionalities of the material increasing the concentration of RH in the test chamber. The electrical conductance and the sensing response of the WO_3 nanostructure as a function of RH are shown in Fig. 4 (a). There is not a significant variation in the conductance of WO_3 with increasing the concentration of RH from 40 to 60%. The conductance value slightly increases (14%) at 80 and 90% of RH. Good stability of electrical conductance of the structure at different RH levels can be attributed to enhanced desorption of water molecules at 400 °C [62,63]. The response of the sensor is reduced by 17% due to the gradual increase of RH in the test chamber from 40 to 90%. Thus, the adsorption of water on WO_3 and hydroxylation of its surface partially affect the electrical conductance of the sensor and its interaction with the analyte molecules. However, the competitive adsorption of water and acetone on the WO_3 surface is a very complex process. In this case, the adsorbed water molecules may affect the formation and the number of oxidized species for the adsorption of acetone [63,64]. Meanwhile, the ionization of water molecules on the surface of the material could be an additional factor partially influencing the response of the sensor [72]. Hence, the small variation in the sensing response of WO_3 with the concentration of RH

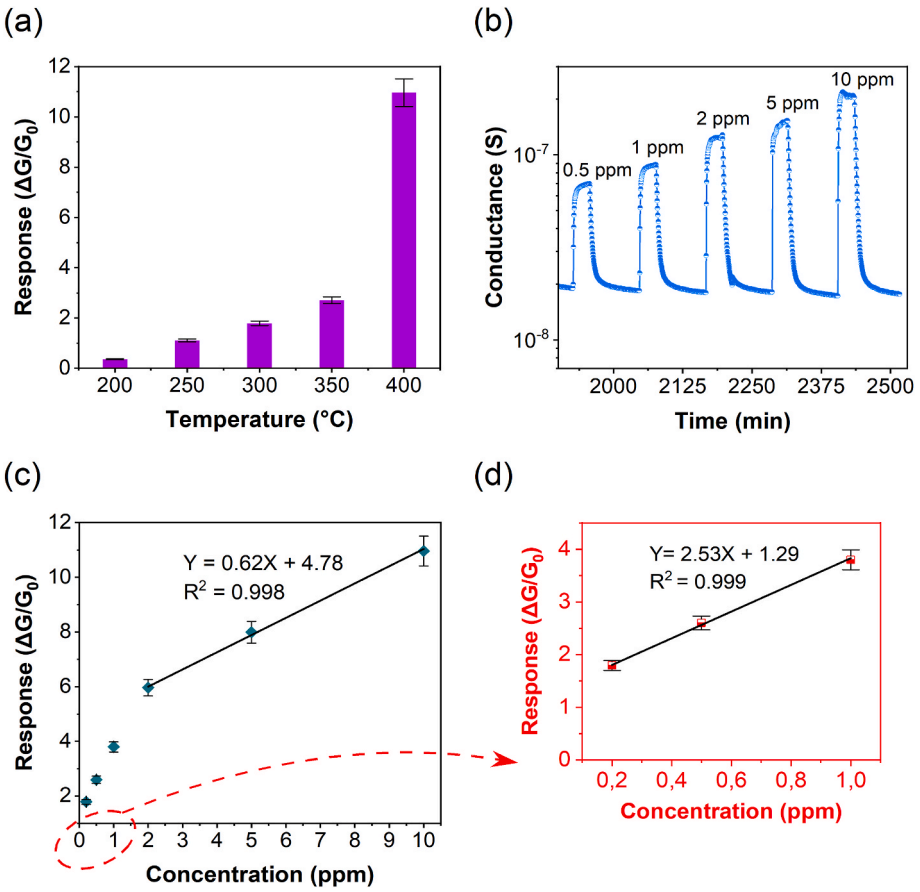

Fig. 3. (a) Acetone sensing response of WO_3 nanomaterial at different temperatures. (b) Dynamic response of the WO_3 gas sensor toward acetone (0.5, 1, 2, 5, and 10 ppm) at 400 °C (RH, 40%). (c) Response of WO_3 toward different concentrations of acetone (0.2–10 ppm) at an operating temperature of 400 °C. (d) A magnified section from figure (c) where the response of the material toward low concentrations of acetone (from 200 ppb to 1 ppm) can be clearly seen.

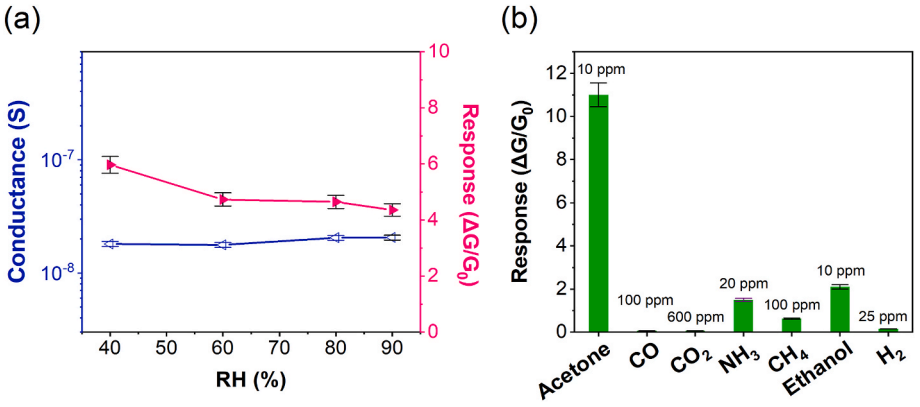

Fig. 4. (a) The variation of the conductance and response values (toward 2 ppm of acetone) of WO_3 depending on the concentration of RH (40–90%) in the test chamber. (b) Respon of WO_3 to acetone, CO, CO_2, NH_3, CH_4, ethanol, and H_2 at 400 °C.

can be attributed to the abovementioned processes.

The ability of a sensing material to determine a specific gaseous compound is an important feature. Therefore, we analyzed the selectivity of the WO_3 sensor to other compounds such as carbon monoxide (CO), carbon dioxide (CO_2), ammonia (NH_3), methane (CH_4), ethanol, and hydrogen (H_2). The obtained results are reported in Fig. 4 (b). The structure is almost not sensitive to CO, CO_2, CH_4, and H_2. Furthermore, its response to 20 ppm of NH_3 (response value: 1.5) and 10 ppm of ethanol (response value: 2.1) is significantly lower compared to 10 ppm of acetone (response value: 11). Thus, the synthesized WO_3 material shows an excellent selective response to acetone. The fabricated monoclinic WO_3 nanostructure (Fig. 2) has a strong interaction with polar molecules of acetone due to its surface acidity and large dipole moment [73–75]. This could be the reason for the high response of the sensor to acetone. Instead, the hexagonal WO_3 is more suitable for the adsorption of CO and CH_4 [76,77]. CO_2 is a linear molecule having a zero dipole moment [78]. The weak interaction of monoclinic WO_3 with CO_2 can be ascribed to the above-mentioned fact [79]. NH_3 and ethanol have smaller dipole moments [80,81]. It has also been demonstrated that the monoclinic WO_3 interacts better with acetone than with ethanol

owing to its surface acidity [82]. Furthermore, the excellent response of monoclinic WO_3 to acetone compared to ethanol, NH_3, and H_2 can be due to differences in adsorption and desorption rates between the material and these gaseous compounds [83,84].

Table S2 reports a comparison between the acetone sensing parameters of the prepared WO_3 nanopowder and other semiconductor structures. Making a direct comparison of sensing structures is difficult, as different experimental setups and test protocols have been used. However, it is worth mentioning that the fabricated WO_3 nanostructure has a good and selective response to acetone without the use of dopants, noble metal catalytic layers, or other additives to functionalize its surface (Table S2). Thus, our findings and the comparison with other metal oxide-based acetone sensors indicate that the monoclinic WO_3 particles owing to their surface acidity and nanodimensions are suitable for the efficient detection of acetone molecules. Furthermore, the sensing tests after 2 months indicate that the WO_3 material has stable functional performance for acetone detection (Fig. S5). Consequently, the obtained results are important for the synthesis of WO_3 nanomaterials using green procedures and their application in acetone sensing devices.

4. Conclusions

We synthesized WO_3 nanopowder by precipitation method using an environmentally friendly solution containing H_2O as the solvent and vitamin C as a surfactant. The morphological analysis of the powder indicates that vitamin C acts as a mild reducing and capping agent in the aqueous solution, resulting in the formation of WO_3 nanoparticles without agglomeration. We also studied the effect of potassium sulfate on particle formation. However, the experimental findings suggest that vitamin C is more effective as a capping agent compared to potassium sulfate. Meanwhile, a further increase in the reaction time can lead to the agglomeration of particles in the aqueous solution of vitamin C. Thus, the reaction time is another significant parameter for the synthesis of WO_3 nanoparticles. Compositional and structural investigations of the prepared nanopowder indicate that it is monoclinic WO_3, which plays a crucial role in its high and selective response to acetone. The enhancement in the sensor response as a function of its operating temperature can be attributed to the improvement of the adsorption of environmental oxygen on the WO_3 surface and required high activation energy for the chemisorption of acetone and its decomposition into CO_2 and H_2O. The fabricated sensing structure is able to detect 200 ppb of acetone without doping or functionalization with specific materials and adding noble metal catalysts. It exhibits a considerably good and stable response to acetone even at 90% of RH. It is expected that the obtained results may be useful for the application of green procedures in the preparation of WO_3 nanomaterials and the development of acetone sensors, as well as other catalytic devices.

Declaration of competing interest

The authors declare that they have no known competing financial interests or personal relationships that could have appeared to influence the work reported in this paper.

Acknowledgements

This study was carried out within the MOST – Sustainable Mobility National Research Center and received funding from the European Union Next-GenerationEU (PIANO NAZIONALE DI RIPRESA E RESILIENZA (PNRR) – MISSIONE 4 COMPONENTE 2, INVESTIMENTO 1.4 – D.D. 1033 17/06/2022, CN00000023), Spoke 5 “Light Vehicle and Active Mobility”. This manuscript reflects only the authors’ views and opinions, neither the European Union nor the European Commission can be considered responsible for them. This work was also sponsored by the “Multi-Messenger and Machine Learning Monitoring of SARS-CoV-2 for occupational health & safety” (4 M SARS-CoV-2) project under the Special Integrative Fund for Research (FISR), Ministry of University and Research (MUR), Italy.

Appendix B. Supplementary data

Supplementary data to this article can be found online at https://doi.org/10.1016/j.ceramint.2023.06.314.

Appendix A. Supplementary data

Supplementary data to this article can be found online at (….).

References

[1] H. Duan, D. Wang, Y. Li, Green chemistry for nanoparticle synthesis, Chem. Soc. Rev. 44 (2015) 5778–5792.
[2] P.T. Anastas, J.C. Warner, Green Chemistry: Theory and Practice, Oxford University Press, 2000.
[3] J.E. Hutchison, Greener nanoscience: a proactive approach to advancing applications and reducing implications of nanotechnology, ACS Nano 2 (2008) 395–402.
[4] J.A. Kumar, T. Krithiga, S. Manigandan, S. Sathish, A.A. Renita, P. Prakash, B.S. N. Prasad, T.R.P. Kumar, M. Rajasimman, A. Hosseini-Bandegharaei, D. Prabu, S. Crispin, A focus to green synthesis of metal/metal based oxide nanoparticles: various mechanisms and applications towards ecological approach, J. Clean. Prod. 324 (2021), 129198.
[5] M.P. Wilson, M.R. Schwarzman, Toward a new U.S. chemicals policy: rebuilding the foundation to advance new science, green chemistry, and environmental health, Environ. Health Perspect. 117 (2009) 1202–1209.
[6] S.S. Mathew, N.E. Sunny, V.K. Shanmugam, Green synthesis of anatase titanium dioxide nanoparticles using Cuminum cyminum seed extract; effect on Mung bean (Vigna radiata) seed germination, Inorg. Chem. Commun. 126 (2021), 108485.
[7] J. Singh, T. Dutta, K.-H. Kim, M. Rawat, P. Samddar, P. Kumar, ‘Green’ synthesis of metals and their oxide nanoparticles: applications for environmental remediation, J. Nanobiotechnol. 16 (2018) 84.
[8] M. Dadkhah, J.-M. Tulliani, Green synthesis of metal oxides semiconductors for gas sensing applications, Sensors 22 (2022) 4669.
[9] J.C. Warner, A.S. Cannon, K.M. Dye, Green chemistry, Environ. Impact Assess. Rev. 24 (2004) 775–799.
[10] M. Choolaei, Q. Cai, B. Amini Horri, Green synthesis and characterisation of nanocrystalline NiO-GDC powders with low activation energy for solid oxide fuel cells, Ceram. Int. 47 (2021) 32804–32816.
[11] A. Sharma, A.K. Saini, N. Kumar, N. Tejwan, T.A. Singh, V.K. Thakur, J. Das, Methods of preparation of metal-doped and hybrid tungsten oxide nanoparticles for anticancer, antibacterial, and biosensing applications, Surface. Interfac. 28 (2022), 101641.
[12] R. Purbia, S. Paria, Green synthesis of single-crystalline akaganeite nanorods for peroxidase mimic colorimetric sensing of ultralow-level vitamin B1 and sulfide ions, ACS Appl. Nano Mater. 1 (2018) 1236–1246.
[13] Y. Tang, Y. Zhao, H. Liu, Room-temperature semiconductor gas sensors: challenges and opportunities, ACS Sens. 7 (2022) 3582–3597.
[14] R.S. Andre, L.A. Mercante, M.H.M. Facure, R.C. Sanfelice, L. Fugikawa-Santos, T. M. Swager, D.S. Correa, Recent progress in amine gas sensors for food quality monitoring: novel architectures for sensing materials and systems, ACS Sens. 7 (2022) 2104–2131.
[15] V. Galstyan, Porous TiO_2-based gas sensors for cyber chemical systems to provide security and medical diagnosis, Sensors 17 (2017).
[16] P. Dutta, G. Gupta, Environmental gas sensors based on electroactive hybrid organic–inorganic nanocomposites using nanostructured materials, Phys. Chem. Chem. Phys. 24 (2022) 28680–28699.
[17] W. Jin, H. Wang, Y. Liu, S. Yang, J. Zhou, W. Chen, SnO_2 quantum dots-functionalized MoO_3 nanobelts for high-selectivity ethylene sensing, ACS Appl. Nano Mater. 5 (2022) 10485–10494.
[18] V. Galstyan, Quantum dots: perspectives in next-generation chemical gas sensors” – A review, Anal. Chim. Acta 1152 (2021), 238192.
[19] V. Galstyan, A. Moumen, G.W.C. Kumarage, E. Comini, Progress towards chemical gas sensors: nanowires and 2D semiconductors, Sensor. Actuator. B Chem. 357 (2022), 131466.
[20] A. Fioravanti, S. Morandi, A.R. Pedrazzo, C. Cecone, M. Manzoli, M. Zanetti, P. Bracco, M. Mazzocchi, S. Lettieri, P. Marani, M.C. Carotta, Investigation of the key parameters for gas sensing through comparison of electrospun and sol-gel semiconducting oxides, Ceram. Int. 48 (2022) 20948–20960.
[21] B. Yuliarto, N.L.W. Septiani, Y.V. Kaneti, M. Iqbal, G. Gumilar, M. Kim, J. Na, K.C. W. Wu, Y. Yamauchi, Green synthesis of metal oxide nanostructures using naturally occurring compounds for energy, environmental, and bio-related applications, New J. Chem. 43 (2019) 15846–15856.
[22] M. Martínez-Cabanas, M. López-García, J.L. Barriada, R. Herrero, M.E. Sastre de Vicente, Green synthesis of iron oxide nanoparticles. Development of magnetic hybrid materials for efficient As(V) removal, Chem. Eng. J. 301 (2016) 83–91.
[23] J. Jeevanandam, S.F. Kiew, S. Boakye-Ansah, S.Y. Lau, A. Barhoum, M.K. Danquah, J. Rodrigues, Green approaches for the synthesis of metal and metal oxide nanoparticles using microbial and plant extracts, Nanoscale 14 (2022) 2534–2571.

[24] S. Poongodi, P.S. Kumar, D. Mangalaraj, N. Ponpandian, P. Meena, Y. Masuda, C. Lee, Electrodeposition of WO_3 nanostructured thin films for electrochromic and H_2S gas sensor applications, J. Alloys Compd. 719 (2017) 71–81.
[25] P. Shandilya, S. Sambyal, R. Sharma, P. Mandyal, B. Fang, Properties, optimized morphologies, and advanced strategies for photocatalytic applications of WO_3 based photocatalysts, J. Hazard Mater. 428 (2022), 128218.
[26] R.S. Vemuri, K.K. Bharathi, S.K. Gullapalli, C.V. Ramana, Effect of structure and size on the electrical properties of nanocrystalline WO_3 films, ACS Appl. Mater. Interfaces 2 (2010) 2623–2628.
[27] E. Spagnoli, B. Fabbri, A. Gaiardo, M. Valt, M. Ardit, S. Krik, G. Cruciani, M. Della Ciana, L. Vanzetti, G. Vola, F. Di Benedetto, A. Migliori, C. Malagù, V. Guidi, Design of a metal-oxide solid solution for selective detection of ethanol with marginal influence by humidity, Sensor. Actuator. B Chem. 370 (2022), 132426.
[28] X. Chang, S. Xu, S. Liu, N. Wang, S. Sun, X. Zhu, J. Li, O. Ola, Y. Zhu, Highly sensitive acetone sensor based on WO_3 nanosheets derived from WS_2 nanoparticles with inorganic fullerene-like structures, Sensor. Actuator. B Chem. 343 (2021), 130135.
[29] G. Zhang, T. Hosomi, W. Mizukami, J. Liu, K. Nagashima, T. Takahashi, M. Kanai, T. Sugiyama, T. Yasui, Y. Aoki, Y. Baba, J.C. Ho, T. Yanagida, A thermally robust and strongly oxidizing surface of WO_3 hydrate nanowires for electrical aldehyde sensing with long-term stability, J. Mater. Chem. 9 (2021) 5815–5824.
[30] I.M. Szilágyi, B. Fórizs, O. Rosseler, Á. Szegedi, P. Németh, P. Király, G. Tárkányi, B. Vajna, K. Varga-Josepovits, K. László, A.L. Tóth, P. Baranyai, M. Leskelä, WO_3 photocatalysts: influence of structure and composition, J. Catal. 294 (2012) 119–127.
[31] S. Americo, E. Pargoletti, R. Soave, F. Cargnoni, M.I. Trioni, G.L. Chiarello, G. Cerrato, G. Cappelletti, Unveiling the acetone sensing mechanism by WO_3 chemiresistors through a joint theory-experiment approach, Electrochim. Acta 371 (2021), 137611.
[32] T. Khalafi, F. Buazar, K. Ghanemi, Phycosynthesis and enhanced photocatalytic activity of zinc oxide nanoparticles toward organosulfur pollutants, Sci. Rep. 9 (2019) 6866.
[33] D. Raoufi, Synthesis and microstructural properties of ZnO nanoparticles prepared by precipitation method, Renew. Energy 50 (2013) 932–937.
[34] R.K. Sharma, R. Ghose, Synthesis of zinc oxide nanoparticles by homogeneous precipitation method and its application in antifungal activity against Candida albicans, Ceram. Int. 41 (2015) 967–975.
[35] M. Nazari, N. Ghasemi, H. Maddah, M.M. Motlagh, Synthesis and characterization of maghemite nanopowders by chemical precipitation method, J. Nanostruct. Chem. 4 (2014) 99.
[36] F. Piccirilli, F. Tardani, A. D'Arco, G. Birarda, L. Vaccari, S. Sennato, S. Casciardi, S. Lupi, Infrared nanospectroscopy reveals DNA structural modifications upon immobilization onto clay nanotubes, Nanomaterials 11 (2021) 1103.
[37] V. Galstyan, A. Ponzoni, I. Kholmanov, M.M. Natile, E. Comini, S. Nematov, G. Sberveglieri, Investigation of reduced graphene oxide and a Nb-doped TiO_2 nanotube hybrid structure to improve the gas-sensing response and selectivity, ACS Sens. 4 (2019) 2094–2100.
[38] X.-L. Li, T.-J. Lou, X.-M. Sun, Y.-D. Li, Highly sensitive WO_3 hollow-sphere gas sensors, Inorg. Chem. 43 (2004) 5442–5449.
[39] J. Xiong, Y. Wang, Q. Xue, X. Wu, Synthesis of highly stable dispersions of nanosized copper particles using l-ascorbic acid, Green Chem. 13 (2011) 900–904.
[40] N.D. Meeks, V. Smuleac, C. Stevens, D. Bhattacharyya, Iron-based nanoparticles for toxic organic degradation: silica platform and green synthesis, Ind. Eng. Chem. Res. 51 (2012) 9581–9590.
[41] F. Ahangaran, A.H. Navarchian, Recent advances in chemical surface modification of metal oxide nanoparticles with silane coupling agents: a review, Adv. Colloid Interface Sci. 286 (2020), 102298.
[42] C. Gutiérrez-Wing, J.J. Velázquez-Salazar, M. José-Yacamán, Procedures for the synthesis and capping of metal nanoparticles, in: M. Soloviev (Ed.), Nanoparticles in Biology and Medicine: Methods and Protocols, Humana Press, Totowa, NJ, 2012, pp. 3–19.
[43] R. Javed, M. Zia, S. Naz, S.O. Aisida, N.u. Ain, Q. Ao, Role of capping agents in the application of nanoparticles in biomedicine and environmental remediation: recent trends and future prospects, J. Nanobiotechnol. 18 (2020) 172.
[44] R.B. Grubbs, Roles of polymer ligands in nanoparticle stabilization, Polym. Rev. 47 (2007) 197–215.
[45] B. Faure, G. Salazar-Alvarez, A. Ahniyaz, I. Villaluenga, G. Berriozabal, Y.R. De Miguel, L. Bergström, Dispersion and surface functionalization of oxide nanoparticles for transparent photocatalytic and UV-protecting coatings and sunscreens, Sci. Technol. Adv. Mater. 14 (2013), 023001.
[46] Y. Zhang, W. Zeng, Y. Li, NO_2 and H_2 sensing properties for urchin-like hexagonal WO_3 based on experimental and first-principle investigations, Ceram. Int. 45 (2019) 6043–6050.
[47] A. Yan, C. Xie, D. Zeng, S. Cai, M. Hu, Synthesis, formation mechanism and sensing properties of WO_3 hydrate nanowire netted-spheres, Mater. Res. Bull. 45 (2010) 1541–1547.
[48] F. Wang, V.N. Richards, S.P. Shields, W.E. Buhro, Kinetics and mechanisms of aggregative nanocrystal growth, Chem. Mater. 26 (2014) 5–21.
[49] W. Li, P. Da, Y. Zhang, Y. Wang, X. Lin, X. Gong, G. Zheng, WO_3 nanoflakes for enhanced photoelectrochemical conversion, ACS Nano 8 (2014) 11770–11777.
[50] Y. Zhang, Y. Wang, L. Zhu, R. Zhang, J. Cao, Enhanced CO sensing performance of WO_3 nanorods with PtAg nanoparticles modification: a combined experimental and first-principle study, Vacuum 193 (2021), 110526.
[51] S. Ansari, M.S. Ansari, S.P. Satsangee, R. Jain, WO_3 decorated graphene nanocomposite based electrochemical sensor: a prospect for the detection of anti-anginal drug, Anal. Chim. Acta 1046 (2019) 99–109.
[52] M. Daniel, B. Desbat, J. Lassegues, B. Gerand, M. Figlarz, Infrared and Raman study of WO_3 tungsten trioxides and WO_3, xH_2O tungsten trioxide tydrates, J. Solid State Chem. 67 (1987) 235–247.
[53] B. Pecquenard, H. Lecacheux, J. Livage, C. Julien, Orthorhombic WO_3 formed via a Ti-stabilized $WO_3{\cdot}13H_2O$ phase, J. Solid State Chem. 135 (1998) 159–168.
[54] Y. Djaoued, S. Balaji, R. Brüning, Electrochromic devices based on porous tungsten oxide thin films, J. Nanomater. 2012 (2012), 674168.
[55] M.H. Mirfasih, C. Li, A. Tayyebi, Q. Cao, J. Yu, J.-J. Delaunay, Oxygen-vacancy-induced photoelectrochemical water oxidation by platelike tungsten oxide photoanodes prepared under acid-mediated hydrothermal treatment conditions, RSC Adv. 7 (2017) 26992–27000.
[56] G. Fulton, A. Lunev, Probing the correlation between phase evolution and growth kinetics in the oxide layers of tungsten using Raman spectroscopy and EBSD, Corrosion Sci. 162 (2020), 108221.
[57] G.N. Kustova, Y.A. Chesalov, L.M. Plyasova, I.Y. Molina, A.I. Nizovskii, Vibrational spectra of $WO_3{\cdot}nH_2O$ and WO_3 polymorphs, Vib. Spectrosc. 55 (2011) 235–240.
[58] C. Balázsi, M. Farkas-Jahnke, I. Kotsis, L. Petrás, J. Pfeifer, The observation of cubic tungsten trioxide at high-temperature dehydration of tungstic acid hydrate, Solid State Ionics 141–142 (2001) 411–416.
[59] M. Gotić, M. Ivanda, S. Popović, S. Musić, Synthesis of tungsten trioxide hydrates and their structural properties, Mater. Sci. Eng., B 77 (2000) 193–201.
[60] F.S. Tehrani, Hydrothermal synthesis and characterization of WO_3 nanostructures: effect of reaction time, Mater. Res. Express 7 (2020).
[61] J.D.-G. Diaz-Reyes, V. Perez-Benitez, A. y Balderas-Lopez, J. A, Obtaining films of tungsten trioxide (WO_3) by resistive heating of a tungsten filament, Superf. vacío 21 (2008) 12–17.
[62] M.J. Madou, S.R. Morrison, 10 - thin-film gas sensors, in: M.J. Madou, S. R. Morrison (Eds.), Chemical Sensing with Solid State Devices, Academic Press, San Diego, 1989, pp. 419–435.
[63] M.J. Madou, S.R. Morrison, 3 - solid/gas interfaces, in: M.J. Madou, S.R. Morrison (Eds.), Chemical Sensing with Solid State Devices, Academic Press, San Diego, 1989, pp. 67–104.
[64] M. Karmakar, B. Mondal, M. Pal, K. Mukherjee, Acetone and ethanol sensing of barium hexaferrite particles: a case study considering the possibilities of non-conventional hexaferrite sensor, Sensor. Actuator. B Chem. 190 (2014) 627–633.
[65] Q. Wang, X. Cheng, Y. Wang, Y. Yang, Q. Su, J. Li, B. An, Y. Luo, Z. Wu, E. Xie, Sea urchins-like WO_3 as a material for resistive acetone gas sensors, Sensor. Actuator. B Chem. 355 (2022), 131262.
[66] X. Zhang, B. Dong, W. Liu, X. Zhou, M. Liu, X. Sun, J. Lv, L. Zhang, W. Xu, X. Bai, L. Xu, S. Mintova, H. Song, Highly sensitive and selective acetone sensor based on three-dimensional ordered WO_3/Au nanocomposite with enhanced performance, Sensor. Actuator. B Chem. 320 (2020), 128405.
[67] W. Zhang, Y. Fan, T. Yuan, B. Lu, Y. Liu, Z. Li, G. Li, Z. Cheng, J. Xu, Ultrafine tungsten oxide nanowires: synthesis and highly selective acetone sensing and mechanism analysis, ACS Appl. Mater. Interfaces 12 (2020) 3755–3763.
[68] M.R. Adib, V.V. Kondalkar, K. Lee, Development of highly sensitive ethane gas sensor based on 3D WO_3 nanocone structure integrated with low-powered in-plane microheater and temperature sensor, Adv. Mater. Technol. 5 (2020), 2000009.
[69] S. Zeb, G. Sun, Y. Nie, Y. Cui, X. Jiang, Synthesis of highly oriented WO_3 nanowire bundles decorated with Au for gas sensing application, Sensor. Actuator. B Chem. 321 (2020), 128439.
[70] R.I. Guzman-Avilan, S.N. González- Diaz, A.A. Cruz, A. Macias-Weinmann, B. E. Villarreal, C. Macouzet-Sanchez, R.V. Villarreal-Gonzalez, C.E.d. Lira-Quezada, K.G. Avilan, D. Sanchez-Guerra, Comparison of exhaled breath fraction temperature (frEBT) in patients with respiratory allergy, J. Allergy Clin. Immunol. 141 (2018) AB98.
[71] H. Schwoebel, R. Schubert, M. Sklorz, S. Kischkel, R. Zimmermann, J.K. Schubert, W. Miekisch, Phase-resolved real-time breath analysis during exercise by means of smart processing of PTR-MS data, Anal. Bioanal. Chem. 401 (2011) 2079.
[72] N. Agmon, The Grotthuss mechanism, Chem. Phys. Lett. 244 (1995) 456–462.
[73] H. Yang, H. Sun, Q. Li, P. Li, K. Song, B. Song, L. Wang, Structural, electronic, optical and lattice dynamic properties of the different WO_3 phases: first-principle calculation, Vacuum 164 (2019) 411–420.
[74] P.M. Woodward, A.W. Sleight, T. Vogt, Ferroelectric tungsten trioxide, J. Solid State Chem. 131 (1997) 9–17.
[75] G.M. Maksimov, G.S. Litvak, A.A. Budneva, E.A. Paukshtis, A.N. Salanov, V. A. Likholobov, WO_3/MO_2 (M = Zr, Sn, Ti) heterogeneous acid catalysts: synthesis, study, and use in cumene hydroperoxide decomposition, Kinet. Catal. 47 (2006) 564–571.
[76] R. Wu, F. Tian, Z. Liu, X. Xue, J. Zhang, J. Zu, CH_4 activation and sensing on hexagonal WO_3 (001) and (110) surfaces, Appl. Surf. Sci. 481 (2019) 1154–1159.
[77] F. Tian, L. Zhao, X.-Y. Xue, Y. Shen, X. Jia, S. Chen, Z. Wang, DFT study of CO sensing mechanism on hexagonal WO_3 (001) surface: the role of oxygen vacancy, Appl. Surf. Sci. 311 (2014) 362–368.
[78] J.S. Muenter, R. Bhattacharjee, The electric dipole moment of the CO_2–CO van der Waals complex, J. Mol. Spectrosc. 190 (1998) 290–293.
[79] Y. Lin, G. Huang, L. Chen, J. Zhang, L. Liu, Enhanced CO_2 photoreduction by Ni $(OH)_2$-x/WO_3 nanofibers with efficient CO_2 activation and charge separation, Adv. Sustain. Syst. 7 (2023), 2200364.
[80] P. Pracna, V. Špirko, W.P. Kraemer, Electric dipole moment function of ammonia, J. Mol. Spectrosc. 136 (1989) 317–332.
[81] B. Li, G. Sauvé, M.C. Iovu, M. Jeffries-El, R. Zhang, J. Cooper, S. Santhanam, L. Schultz, J.C. Revelli, A.G. Kusne, T. Kowalewski, J.L. Snyder, L.E. Weiss, G. K. Fedder, R.D. McCullough, D.N. Lambeth, Volatile organic compound detection using nanostructured copolymers, Nano Lett. 6 (2006) 1598–1602.

[82] J. Kaur, K. Anand, A. Kaur, R.C. Singh, Sensitive and selective acetone sensor based on Gd doped WO_3/reduced graphene oxide nanocomposite, Sensor. Actuator. B Chem. 258 (2018) 1022–1035.
[83] T.K. Takeo Hyodo, Taro Ueda, Kuniyuki izawa, and yasuhiro shimizu, acetone-sensing properties of WO_3-based gas sensors operated in dynamic temperature modulation mode —effects of loading of noble metal and/or NiO onto WO_3, Sensor. Mater. 28 (2016) 1179–1189.
[84] A.K. Nayak, R. Ghosh, S. Santra, P.K. Guha, D. Pradhan, Hierarchical nanostructured WO_3–SnO_2 for selective sensing of volatile organic compounds, Nanoscale 7 (2015) 12460–12473.